Chapter 13
External Fields

Abstract The effects of external electric and magnetic fields on the electronic and optical properties of bulk materials and quantum wells are discussed including the Stark effect and quantum-confined Stark effect, the Hall effect and Quantized Hall Effects.

13.1 Electric Fields

13.1.1 Bulk Material

The center-of-mass motion of the exciton is not influenced by an electric field. The Hamilton operator for the relative motion of an electron–hole pair of reduced mass μ along z in the presence of an electric field E along the z direction is

$$\hat{H} = -\frac{\hbar^2}{2\mu}\,\Delta - e\,E\,z. \tag{13.1}$$

Here, the Coulomb interaction, leading to the formation of bound exciton states, is neglected. In the plane perpendicular to the field (here the z direction) the solutions for the relative motion are just plane waves.

In the electric field the bands are tilted (Fig. 13.1), i.e. there is no longer an overall band gap. Accordingly, the wavefunctions are modified and have exponential tails in the energy gap.

M. Grundmann, *The Physics of Semiconductors*, Graduate Texts in Physics,
DOI 10.1007/978-3-319-23880-7_13

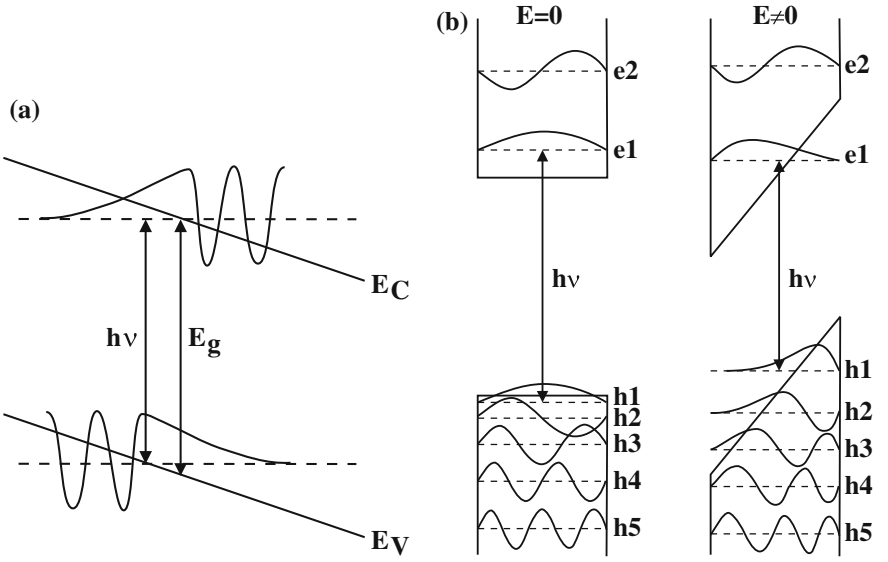

Fig. 13.1 Impact of an electric field on (**a**) bulk material (tilt of bands) and (**b**) a quantum well (quantum confined Stark effect, QCSE)

After separation of the motion in the (x,y) plane the Schrödinger equation for the motion in the z direction is

$$\left(-\frac{\hbar^2}{2\mu}\frac{\mathrm{d}^2}{\mathrm{d}z^2} - e\,E\,z - E_z\right)\phi(z) = 0\,, \tag{13.2}$$

which is of the type

$$\frac{\mathrm{d}^2 f(\xi)}{\mathrm{d}\xi^2} - \xi f(\xi) = 0\,, \tag{13.3}$$

with $\xi = \frac{E_z}{\Theta} - z\left(\frac{2\mu}{\hbar^2}\,e\,E\right)^{1/3}$ and the optoelectronic energy $\Theta = \left(\frac{e^2E^2\hbar^2}{2\mu}\right)^{1/3}$. The solution of (13.3) is given by the Airy function Ai (cf. Fig. 13.2):

$$\phi_{E_z}(\xi) = \frac{\sqrt{e\,E}}{\Theta}\,Ai(\xi). \tag{13.4}$$

The pre-factor guaranties the orthonormality (with regard to the E_z). The absorption spectrum is then given by

$$\alpha(\omega, E) \propto \frac{1}{\omega}\sqrt{\Theta}\,\pi\left[Ai'^2(\eta) - \eta\,Ai^2(\eta)\right]\,, \tag{13.5}$$

with $\eta = (E_\mathrm{g} - E)/\Theta$ and $Ai'(x) = \mathrm{d}Ai(x)/\mathrm{d}x$.

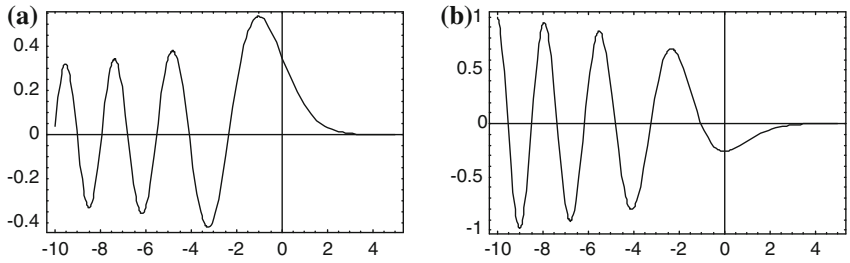

Fig. 13.2 (**a**) Airy function Ai(x), (**b**) Ai'(x)

Optical transitions below the band gap become possible that are photon-assisted tunneling processes. The below-bandgap transitions have the form of an exponential tail. Additionally, oscillations develop above the band gap, the so-called Franz–Keldysh oscillations (FKO) (Fig. 13.3a).

The absorption spectrum scales with the optoelectronic energy Θ. The energy position of the FKO peaks E_n is periodic with ($\nu \sim 0.5$)

$$\left(E_n - E_g\right)^{3/2} \propto (n - \nu)\, E\, \sqrt{\mu}. \tag{13.6}$$

A nonperiodicity can indicate a nonparabolicity of the mass. For a given mass the electric field strength can be determined. Well-pronounced oscillations are only present for homogeneous fields.

Experimental spectra show additionally the peaks due to excitonic correlation (Fig. 13.3b) at low field strength. At higher fields the FKO evolve and the amplitude of the excitonic peaks decreases because the excitons are ionized in the field.

13.1.2 Quantum Wells

In a quantum well an electric field along the confinement direction (z direction) causes electrons and holes to shift their mean position to opposite interfaces (Fig. 13.1b). However, excitons are not ionized due to the electric field. With increasing field (for both field directions) the energy position of the absorption edge and the recombination energy is reduced. This is the quantum confined Stark effect (QCSE). Corresponding experimental data are shown in Fig. 13.4i–v. The shift depends quadratically on the electric field since the exciton has no permanent dipole moment (mirror symmetry of the quantum well). Thus, only the second-order Stark effect is present (as for the hydrogen atom) in which the field first induces a dipole $\mathbf{p} = \alpha\mathbf{E}$. This dipole interacts with the field with an energy $E = -\mathbf{p}\cdot\mathbf{E} = -\alpha\mathbf{E}^2$. The carrier separation in opposite sides of the quantum well (Fig. 13.4b) leads to a reduced overlap of the electron and hole wavefunctions and subsequently to an increased recombination lifetime (see Fig. 12.42).

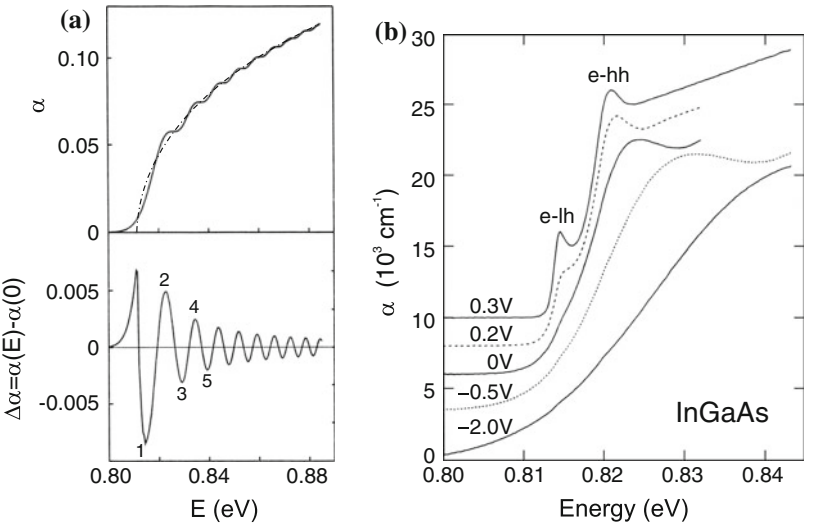

Fig. 13.3 (**a**) Theoretical absorption (*top panel*) with (*solid line*) and without (*dash-dotted line*) electric field for a volume semiconductor (without Coulomb interaction) and theoretical change of absorption (*bottom panel*). (**b**) Experimental absorption spectra of InGaAs on InP at $T = 15\,\mathrm{K}$ for various applied voltages as labeled. Adapted from [1081]

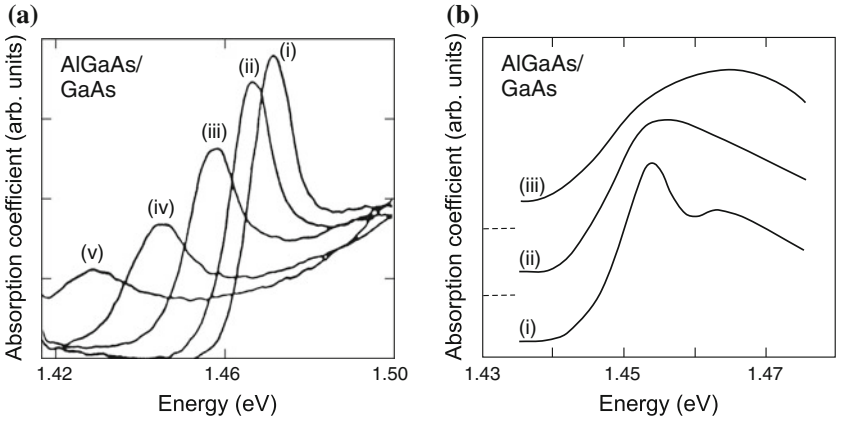

Fig. 13.4 Impact of electric fields on the absorption spectrum of $n \times$ (9.5 nm GaAs/9.8 nm $Al_{0.32}Ga_{0.68}As$) multiple quantum well structures. **a** Electric field along the [001] growth direction ($n = 50$), (**i**)–(**v**): $E = 0$, 0.6, 1.1, 1.5, and 2×10^5 V/cm. **b** Electric field within the interface plane (n = 60), (**i**–**iii**): $E = 0$, 1.1, and 2×10^5 V/cm. Adapted from [1082]

If the field is within the quantum-well interface plane, the field leads to the ionization of excitons without shift of the energy position. The loss of the excitonic peak is visualized in the spectra in Fig. 13.4a–c.

13.2 Magnetic Fields

In magnetic fields, electrons (or holes) perform a cyclotron motion with frequency $\omega_c = eB/m^*$, i.e. a motion perpendicular to the magnetic field on a line of constant energy in **k**-space. This line is the intersection of a plane perpendicular to the magnetic field and the respective isoenergy surface in **k**-space. For semiconductors with anisotropic mass, such as Si and Ge, the quantum theory of cyclotron resonance has been given in [1083]. The physics of semiconductors in magnetic fields is covered in detail in [1084].

The ballistic cyclotron motion can only occur between two scattering events. Thus, a significantly long path along the cyclotron trajectory (classically speaking) and the connected magnetotransport properties are only possible when

- $\omega_c \tau \gg 1$, i.e. when the average scattering time τ is sufficiently large. This requires high mobility.
- the magnetic field is sufficiently strong and the temperature sufficiently low, i.e. $\hbar\omega_c \gg kT$, such that thermal excitations do not scatter electrons between different Landau levels.
- the cyclotron path is free of geometric obstructions.

An external magnetic field also produces a splitting of the spin states. For the electron, the energy splitting ΔE is given by

$$\Delta E = g_e^* \mu_B B \,, \tag{13.7}$$

where B is the magnetic-field amplitude and g_e^* the (effective) electron g-factor. This value differs from the free-electron value in vacuum of $g_e = 2.0023$ due to the presence of spin-orbit interaction (see Sect. 13.2.3). Values for g_e^* at low carrier density and low temperatures are 2 for Si, 1.2 for InP and ZnSe, -1.65 for CdTe, -0.44 for GaAs, -15 in InAs, and -50 for InSb. In [1085] the temperature dependence of g_e^* in GaAs, InP and CdTe is also measured and discussed. The electron g-factor increases in thin GaAs/AlGaAs quantum wells [1086].

13.2.1 Hall Effect

An electrical current along the x (longitudinal) direction in a perpendicular magnetic field $\mathbf{B} = (0, 0, B)$ along z causes an electric field E_y along the transverse (y) direction (Fig. 13.5). The charge accumulation is due to the Lorentz force. The related

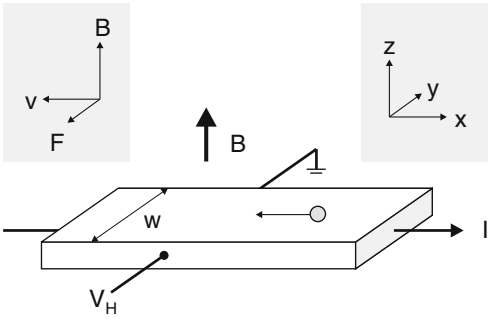

Fig. 13.5 Scheme of the Hall-effect geometry. The movement of one electron in the longitudinal electric current I is shown schematically. The coordinate system (x, y, z) and the directions of the magnetic field $\mathbf{B}$, the drift velocity of an electron $\mathbf{v}$ and the resulting Lorentz force $\mathbf{F}$ are given. The transverse field E_y is given by V_H/w

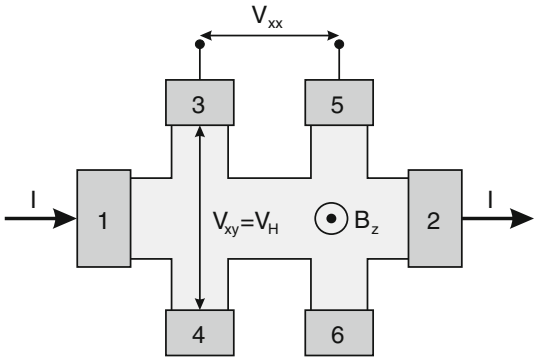

Fig. 13.6 Hallbar geometry. The current I is driven by a source from contact 1 to 2. The Hall voltage is measured between contacts 3 and 4, the longitudinal voltage between 3 and 5

transverse voltage is called the Hall voltage and the resistivity $\rho_{xy} = E_y/j_x$ the Hall resistivity [21, 24, 25]. Many aspects of the Hall effect are discussed in [1087]. For thin-film samples typically Hall bars [1088] (see Fig. 13.6 and also Fig. 13.17, for a reasonable measurement of the Hall voltage the ratio of length and width of the Hall bar should be at least 3) or the van-der-Pauw geometry (Fig. 13.7) and method are used [1089–1091].

For band transport in the relaxation time approximation (Sect. 8.2), the steady-state equation of motion is

$$m^* \frac{\mathbf{v}}{\tau} = q\ (\mathbf{E} + \mathbf{v} \times \mathbf{B})\,. \tag{13.8}$$

We note that this equation of motion is also valid for holes, given the convention of Sect. 6.9.1, i.e. positive effective mass and charge. With the cyclotron frequency $\omega_\mathrm{c} = qB/m^*$ the conductivity tensor is ($\mathbf{j} = qn\mathbf{v} = \boldsymbol{\sigma}\,\mathbf{E}$)

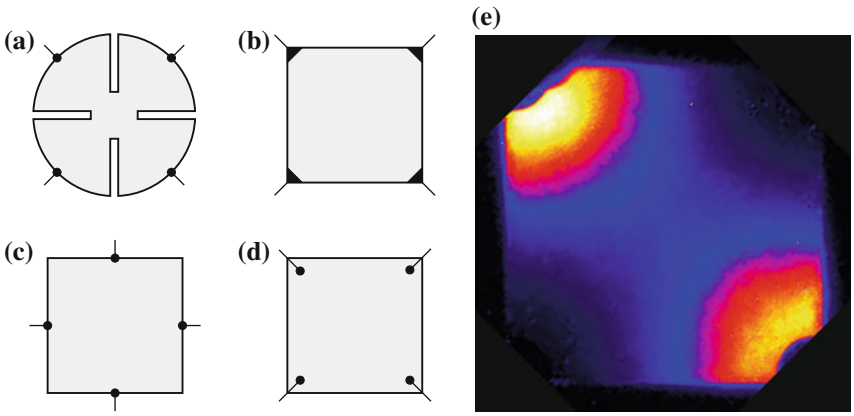

Fig. 13.7 (**a**–**d**) Geometry for van-der-Pauw Hall measurements. (**a**) Best geometry (*cloverleaf*), (**b**) acceptable square geometry with small contacts on the corners, (**c**,**d**) not recommended geometries with contacts on the edge centers or inside the square, respectively. (**e**) Current distribution, as visualized by lock-in thermography [1092], in epitaxial ZnO layer on sapphire with Hall geometry as in part (**b**). *Grey dashed line* indicates the outline of the $10 \times 10\,\mathrm{mm}^2$ substrate, *grey areas* indicate gold ohmic contacts

$$\boldsymbol{\sigma} = \begin{pmatrix} \sigma_{xx} & \sigma_{xy} & 0 \\ \sigma_{yx} & \sigma_{yy} & 0 \\ 0 & 0 & \sigma_{zz} \end{pmatrix} \tag{13.9a}$$

$$\sigma_{xx} = \sigma_{yy} = \sigma_0 \frac{1}{1 + \omega_c^2 \tau^2} = \sigma_0 \frac{1}{1 + \mu^2 B^2} \tag{13.9b}$$

$$\sigma_{xy} = -\sigma_{yx} = \sigma_0 \frac{\omega_c \tau}{1 + \omega_c^2 \tau^2} = \sigma_0 \frac{\mu B}{1 + \mu^2 B^2} \tag{13.9c}$$

$$\sigma_{zz} = \sigma_0 = \frac{q^2 n \tau}{m^*} = q n \mu. \tag{13.9d}$$

Perpendicular to the magnetic field, the conductivity (σ_{zz}) is given by (8.5). If only one type of carrier (charge q, density n) is considered, the condition $j_y = 0$ leads to $E_y = \mu B E_x$ and $j_x = \sigma_0 E_x$. The Hall coefficient is defined as $R_\mathrm{H} = E_y/(j_x B)$ or more precisely as

$$R_\mathrm{H} = \frac{\rho_{xy}}{B}\,, \tag{13.10}$$

where the resistivity tensor $\boldsymbol{\rho}$ is the inverse of the conductivity tensor $\boldsymbol{\sigma}$,

$$\boldsymbol{\rho} = \boldsymbol{\sigma}^{-1} = \begin{pmatrix} \rho_{xx} & \rho_{xy} & 0 \\ \rho_{yx} & \rho_{yy} & 0 \\ 0 & 0 & \rho_{zz} \end{pmatrix} \tag{13.11a}$$

$$\rho_{xx} = \rho_{yy} = \frac{\sigma_{xx}}{\sigma_{xx}^2 + \sigma_{xy}^2} \tag{13.11b}$$

$$\rho_{xy} = -\rho_{yx} = \frac{\sigma_{xy}}{\sigma_{xx}^2 + \sigma_{xy}^2} \tag{13.11c}$$

$$\rho_{zz} = \frac{1}{\sigma_{zz}} = \frac{1}{\sigma_0}. \tag{13.11d}$$

For a single type of carriers, the Hall coefficient is therefore given by

$$R_\mathrm{H} = \frac{\mu}{\sigma_0} = \frac{1}{q\,n}. \tag{13.12}$$

It is negative (positive) for electron (hole) conduction. We note that electrons and holes are deflected in the *same* y-direction by the magnetic field and collect at the same electrode. Thus the Hall effect allows the determination of the carrier type and the carrier density.[1]

If both types of carriers are present simultaneously, the conductivity (two-band conduction) is given by the sum of electron and hole conductivity (8.11),

$$\boldsymbol{\sigma} = \boldsymbol{\sigma}_\mathrm{e} + \boldsymbol{\sigma}_\mathrm{h}. \tag{13.13}$$

The Hall constant (13.10) is then

$$R_\mathrm{H} = \frac{1}{e}\,\frac{-n\,\mu_\mathrm{e}^2\,(1+\mu_\mathrm{h}^2\,B^2) + p\,\mu_\mathrm{h}^2\,(1+\mu_\mathrm{e}^2\,B^2)}{n^2\,\mu_\mathrm{e}^2\,(1+\mu_\mathrm{h}^2\,B^2) - 2\,n\,p\,\mu_\mathrm{e}\,\mu_\mathrm{h}\,(1+\mu_\mathrm{e}\,\mu_\mathrm{h}\,B^2) + p^2\,\mu_\mathrm{h}^2\,(1+\mu_\mathrm{e}^2\,B^2)}. \tag{13.14}$$

Under the assumption of small magnetic fields,[2] i.e. $\mu B \ll 1$, the Hall coefficient is

$$R_\mathrm{H} = \frac{1}{e}\left[\frac{-n\,\mu_\mathrm{e}^2 + p\,\mu_\mathrm{h}^2}{(-n\,\mu_\mathrm{e} + p\,\mu_\mathrm{h})^2} + \frac{n\,p\,(-n+p)\,\mu_\mathrm{e}^2\,\mu_\mathrm{h}^2\,(\mu_\mathrm{e}-\mu_\mathrm{h})^2}{(-n\,\mu_\mathrm{e} + p\,\mu_\mathrm{h})^4}\,B^2 + \cdots\right]. \tag{13.15}$$

For small magnetic field this can be written as

$$R_\mathrm{H} = \frac{1}{e}\,\frac{p - n\,\beta^2}{(p - n\,\beta)^2}\ , \tag{13.16}$$

[1] Using the Hall effect, the net *free* charge carrier concentration is determined. We note that the concentration of *fixed* charges in semiconductors can be investigated by depletion layer spectroscopy (Sect. 21.2.4).

[2] We note that for a mobility of $10^4\,\mathrm{cm^2/Vs}$, μ^{-1} is a field of $B = 1\,\mathrm{T}$.

with $\beta = \mu_e/\mu_h < 0$. For large magnetic fields, i.e. $\mu B \gg 1$, the Hall coefficient is given by

$$R_H = \frac{1}{e}\frac{1}{p-n}. \tag{13.17}$$

In Fig. 13.8, the absolute value of the Hall coefficient for InSb samples with different doping concentrations is shown. The p-doped samples exhibit a reverse of the sign of the Hall coefficient upon increase of temperature when intrinsic electrons contribute to the conductivity. The zero in R_H occurs for $n = p\,\mu_h^2/\mu_e^2 = n_i/|\beta|$. For high temperatures, the Hall coefficient for n- and p-doped samples is dominated by the electrons that have much higher mobility (Table 8.2).

The simultaneous conduction in a band and an impurity band (cmp. Sect. 7.5.7) has been separated with a suitable model assuming two conduction channels for holes [1094] (Fig. 13.9).

In the derivation of the (unipolar) Hall coefficient we had assumed that all carriers involved in the transport have the same properties, in particular that they are subject to the same scattering time. This assumption is generally not the case (cmp. Appendix I) and we need to operate with the ensemble average of the discussed

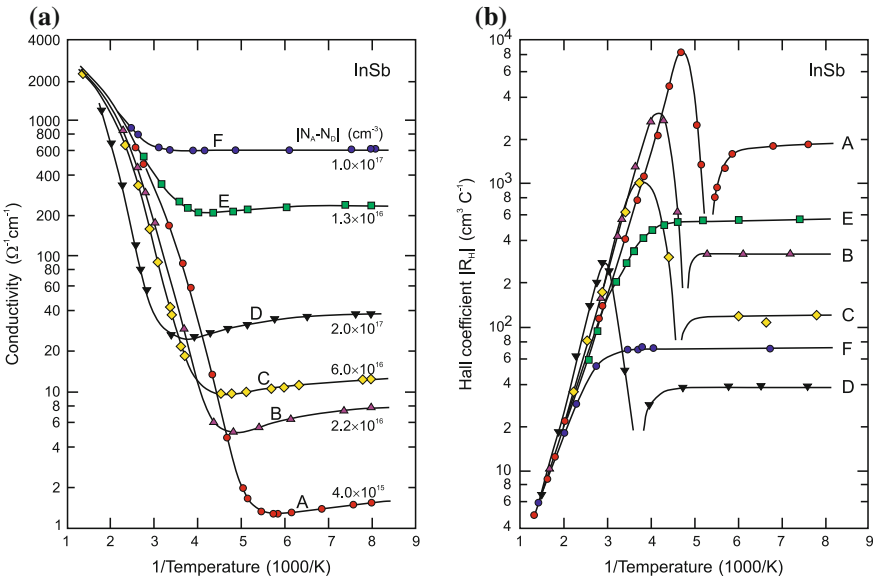

Fig. 13.8 (**a**) Conductivity and (**b**) absolute value of the Hall coefficient versus inverse temperature for four p-doped (A–D) and two n-doped (E, F) InSb samples. The doping levels are given in (**a**). Adapted from [1093]

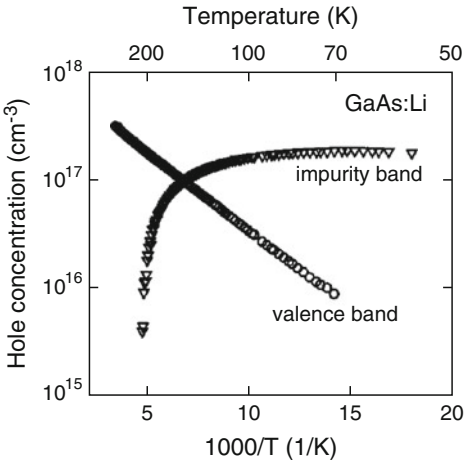

Fig. 13.9 Carrier densities in valence band (*circles*) and impurity band (*triangles*) from evaluating the Hall effect on GaAs doped with lithium (and annealed) taking into account two conduction channels. Adapted from [1094]

quantities. The ensemble average of an energy-dependent quantity $\zeta(E)$ over the (electron) distribution function $f(E)$ is denoted as $\langle\zeta\rangle$ and is given as[3]

$$\langle\zeta\rangle = \frac{\int \zeta(e) f(E)\,\mathrm{d}E}{\int f(E)\,\mathrm{d}E}. \tag{13.18}$$

In particular $\langle\tau\rangle^2$ is now different from $\langle\tau^2\rangle$. Considering the equation $\langle\mathbf{j}\rangle = \langle\boldsymbol{\sigma}\rangle\,\mathbf{E}$ for the ensemble averaged current densities we find (for one type of carrier, cf. (13.12))

$$R_\mathrm{H} = \frac{1}{q\,n}\,r_\mathrm{H}\,, \tag{13.19}$$

with the so-called *Hall factor* r_H given by

$$\begin{aligned} r_\mathrm{H} &= \frac{\gamma}{\alpha^2 + \omega_\mathrm{c}^2\,\gamma^2} \\ \alpha &= \langle\frac{\tau}{1+\omega_\mathrm{c}^2\,\tau^2}\rangle \\ \gamma &= \langle\frac{\tau^2}{1+\omega_\mathrm{c}^2\,\tau^2}\rangle. \end{aligned} \tag{13.20}$$

[3]For this consideration it is assumed that the energy dependence is the decisive one. Generally, averaging may have to be performed over other degrees of freedom as well, such as the spin or, in the case of anisotropic bands, the orbital direction.

The Hall factor depends on the scattering mechanisms and is of the order of 1. For large magnetic fields the Hall factor approaches 1. For small magnetic fields we have

$$R_{\mathrm{H}} = \frac{1}{q\,n}\,\frac{\langle\tau^2\rangle}{\langle\tau\rangle^2}. \tag{13.21}$$

The mobility calculated from (cf. (13.9d)) $\sigma_0 R_{\mathrm{H}}$ is called the *Hall mobility* μ_{H} and is related to the mobility via

$$\mu_{\mathrm{H}} = r_{\mathrm{H}}\,\mu. \tag{13.22}$$

It is assumed so far that the free carrier density and mobility are homogeneous within the volume of current transport. Multi-layer models can be fitted to experimental Hall data in order to account for different conduction channels in different layered parts of the sample [1095]. E.g., in a two-layer model, contributions from bulk and surface/interface conduction can be separated [1096–1098].

The magnetic field dependence of $\boldsymbol{\sigma}$ can be used in a general case to separate contributions of carriers with different density and mobility (including its sign) without assumptions and obtain the mobility spectrum $s(\mu)$ (MSA, mobility spectral analysis),

$$\sigma_{xx} = \int_{-\infty}^{\infty} s(\mu)\,\frac{1}{1+\mu^2B^2}\,\mathrm{d}\mu \tag{13.23a}$$

$$\sigma_{xy} = \int_{-\infty}^{\infty} s(\mu)\,\frac{\mu B}{1+\mu^2B^2}\,\mathrm{d}\mu, \tag{13.23b}$$

as a generalization of (13.13), (13.9b) and (13.9c) [1099-1101]. Examples are the separation of electron conductivity in (GaAs-) Γ- and (InAs-) X-Minima in a GaAs/AlGaAs/InAs double quantum well structures [1099] (Fig. 13.10a), substrate and 2DEG electron conductivity in AlGaN/GaN heterostructures [1102], and electrons and holes in an InAs/GaSb quantum well [1100] (Fig. 13.10b).

In the case of hopping conduction (Sect. 8.7), the theory of Hall effect is more involved [1103, 1104]. If carriers are transported by hopping, generally, they may not be free to move as expected by (13.8) in response to the applied magnetic field and the Lorentz force. A Hall effect occurs only at the junction of *three* (or more) hopping sites [1103]. The sign of the experimentally determined Hall coefficient is often opposite to the one expected from the carrier type according to (13.12), e.g. as studied in a-Si [1105, 1106]. The *sign anomaly* depends on intricacies such as the local site geometry and interference processes taking place among bonding and antibonding orbitals of various numbers as summarized in [1107].

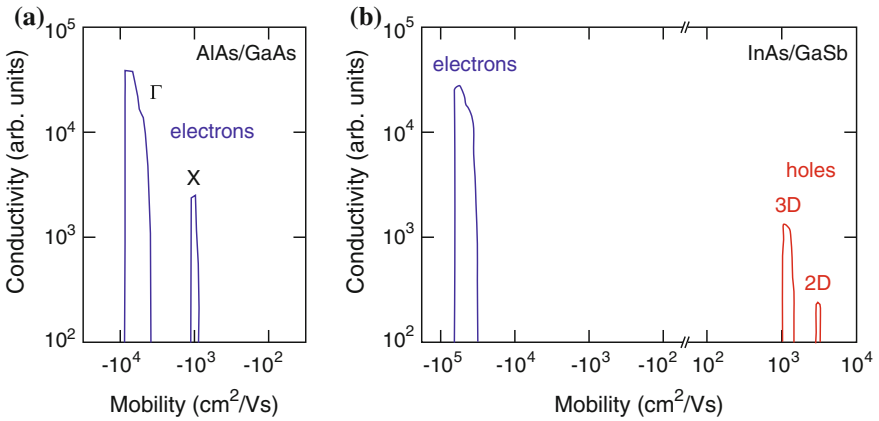

Fig. 13.10 (**a**) Mobility spectrum of GaAs/AlGaAs/InAs double quantum well structure. Adapted from [1099]. (**b**) Mobility spectrum of InAs/GaSb quantum well structure. Adapted from [1100]

13.2.2 Free-Carrier Absorption

The absorption of free carriers was treated in Sect. 9.8.1 without the presence of a static magnetic field. Solving (13.8) for a static magnetic field $\mathbf{B} = \mu_0 \mathbf{H}$ with $\mathbf{H} = H(h_x, h_y, h_z)$ and a harmonic electric field $\mathbf{E} \propto \exp(-\mathrm{i}\omega t)$ yields for the dielectric tensor (cf. (9.60))

$$\boldsymbol{\epsilon} = \frac{\mathrm{i}}{\epsilon_0 \, \omega} \boldsymbol{\sigma}, \tag{13.24}$$

and by comparing to $\mathbf{j} = \boldsymbol{\sigma} \, \mathbf{E} = q \, n \, \mathbf{v}$,

$$\boldsymbol{\epsilon}(\omega) = -\omega_\mathrm{p}^{*2} \left[(\omega^2 + \mathrm{i}\,\omega\,\gamma)\,\mathbf{1} - \mathrm{i}\,\omega_\mathrm{c} \begin{pmatrix} 0 & -h_z & h_y \\ h_z & 0 & -h_x \\ -h_y & h_x & 0 \end{pmatrix} \right]^{-1}, \tag{13.25}$$

where $\mathbf{1}$ denotes the (3 by 3) unity matrix and $\gamma = 1/\tau = q/(m^* \mu)$ is the damping parameter with μ representing the optical carrier mobility (in the non-isotropic case a tensor $\boldsymbol{\gamma}$ needs to be used). The (unscreened) plasma frequency is given by (cmp. (9.65))

$$\omega_\mathrm{p}^* = \sqrt{n \, \frac{e^2}{\epsilon_0 \, m^*}}. \tag{13.26}$$

The free-carrier cyclotron frequency is

$$\omega_\mathrm{c} = e\,\frac{\mu_0 H}{m^*}. \tag{13.27}$$

If the effective mass is treated as a tensor, $1/m^*$ is replaced by $\mathbf{m}^{*-1}$ in (13.26) and (13.27). For zero magnetic field the classical Drude theory for one carrier species is recovered (cf. (9.62a))

$$\boldsymbol{\epsilon}(\omega) = -\frac{\omega_\mathrm{p}^{*2}}{\omega\,(\omega + \mathrm{i}\gamma)}. \tag{13.28}$$

With the magnetic field perpendicular to the sample surface, i.e. $\mathbf{B} = \mu_0\,(0, 0, H)$ the magneto-optic dielectric tensor simplifies to (cf. (13.9d))

$$\boldsymbol{\epsilon}(\omega) = -\frac{\omega_\mathrm{p}^{*2}}{\omega^2}\begin{pmatrix} \tilde{\epsilon}_{xx} & \mathrm{i}\tilde{\epsilon}_{xy} & 0 \\ -\mathrm{i}\tilde{\epsilon}_{xy} & \tilde{\epsilon}_{xx} & 0 \\ 0 & 0 & \tilde{\epsilon}_{zz} \end{pmatrix} \tag{13.29a}$$

$$\tilde{\epsilon}_{xx} = \frac{1 + \mathrm{i}\gamma/\omega}{(1 + \mathrm{i}\gamma/\omega)^2 - (\omega_\mathrm{c}/\omega)^2} \tag{13.29b}$$

$$\tilde{\epsilon}_{zz} = \frac{1}{(1 + \mathrm{i}\gamma/\omega)} \tag{13.29c}$$

$$\tilde{\epsilon}_{xy} = \frac{\omega_\mathrm{c}/\omega}{(1 + \mathrm{i}\gamma/\omega)^2 - (\omega_\mathrm{c}/\omega)^2}. \tag{13.29d}$$

The in-plane component ϵ_{xx} provides information about ω_p^* and γ, i.e. two of the three parameters n, μ and m^* are known. Additionally, the antisymmetric tensor component ϵ_{xy} is linear in the cyclotron frequency and provides q/m^*. This subtle but finite birefringence depends on the strength (and orientation) of the magnetic field and can be experimentally determined in the infrared using magneto-ellipsometry [1108, 1109]. Such 'optical Hall effect' experiment allows the determination of the carrier density n, the mobility μ, the carrier mass[4] m^* and the sign of the carrier charge $\mathrm{sgn}(q)$ with optical means. The electrical Hall effect (Sect. 13.2.1) can reveal n, μ and $\mathrm{sgn}(q)$ but cannot reveal the carrier mass.

13.2.3 Energy Levels in Bulk Crystals

In a 3D electron gas (the magnetic field is along z, i.e. $\mathbf{B} = B[0, 0, 1]$) the motion in the (x, y) plane is described by Landau levels. Quantum mechanically they correspond to levels of a harmonic oscillator. The magnetic field has no impact on

[4] We note that mobility and effective mass defined and measured in this way may be referred to as 'optical'. Other definitions and approaches to the mobility or effective mass may give different results.

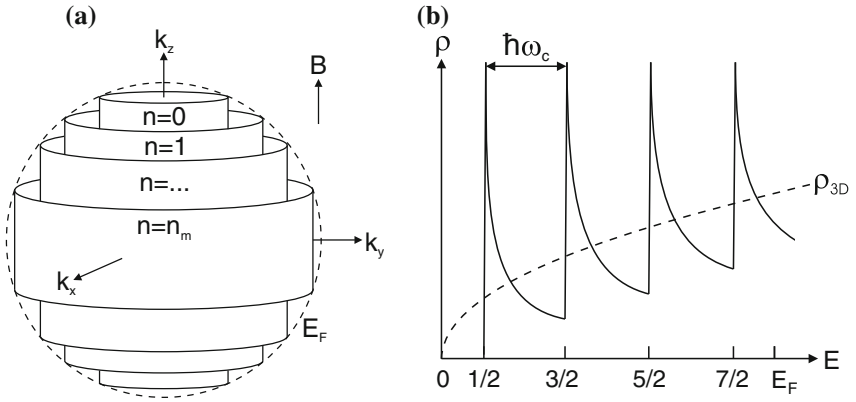

Fig. 13.11 3D electron gas in an external magnetic field. (**a**) Allowed states in **k**-space for magnetic field along the z direction. (**b**) Density of states (DOS) ρ versus energy (in units of $\hbar\omega_c$). *Dashed line* is three-dimensional DOS without magnetic field. Based on [991]

the motion of electrons along z, such that in this direction a free dispersion relation $\propto k_z^2$ is present. The energy levels are given as

$$E_{nk_z} = \left(n + \frac{1}{2}\right)\hbar\omega_c + \frac{\hbar^2}{2m}k_z^2. \tag{13.30}$$

Thus, the states are on concentric cylinders in **k**-space (Fig. 13.11a). The populated states of the 3D electron gas (at 0 K) lie within the Fermi vector of length k_F. For the 3D system the density of states at the Fermi energy is a square root function of the Fermi energy (6.67). In the presence of a magnetic field the density of states diverges every time that a new cylinder (with a one-dimensional density of states, (6.75)) touches the Fermi surface at E_F. In real systems, the divergence will be smoothed, however, a pronounced peak or the periodic nature of the density of states is often preserved.

The period is given by the number n_m of cyclotron orbits (Landau levels) within the Fermi surface.

$$\left(n_m + \frac{1}{2}\right)\hbar\omega_c = E_F. \tag{13.31}$$

If the number of carriers is constant, the density of states at the Fermi energy at varying magnetic field varies periodically with $1/B$. From the conditions $\left(n_m + \frac{1}{2}\right)\hbar\frac{eB_1}{m} = E_F$ and $\left(n_m + 1 + \frac{1}{2}\right)\hbar\frac{eB_2}{m} = E_F$ with $\frac{1}{B_2} = \frac{1}{B_1} + \frac{1}{\Delta B}$ we find

$$\frac{1}{\Delta B} = \frac{e\hbar}{m^* E_F}. \tag{13.32}$$

This periodicity is used to determine experimentally, e.g., the properties of the Fermi surface in metals using the Shubnikov–de Haas oscillations (of the magnetoresistance) or the de Haas–van Alphén effect (oscillation of the magnetic susceptibility).

Equation (13.30) needs to be extended to account for the splitting (13.7) of the Landau level due to the electron spin. According to [1110] the electron Landau level energy can be written as

$$E_n = \left(n + \frac{1}{2}\right) \frac{\hbar e B}{m^*(E)} \pm g_e^*(E)\, \mu_B\, B\ , \tag{13.33}$$

with energy dependent effective mass and g-factor

$$\frac{1}{m^*(E)} = \frac{1}{m^*(0)} \frac{E_g\,(E_g + \Delta_0)}{3E_g + 2\Delta_0} \left(\frac{2}{E + E_g} + \frac{1}{E + E_g + \Delta_0}\right) \tag{13.34a}$$

$$g_e^*(E) = g_e^*(0) \frac{E_g(E_g + \Delta_0)}{\Delta_0} \left(\frac{1}{E + E_g} - \frac{1}{E + E_g + \Delta_0}\right) \tag{13.34b}$$

The band edge value $m^*(0)$ of the effective mass is given by (6.39) and that of the g-factor by

$$g_e^*(0) = 2\left[1 - \frac{2\,\Delta_0}{3\,E_g\,(E_g + \Delta_0)} E_P\right]. \tag{13.35}$$

For large spin-orbit splitting, the value of the g-factor deviates strongly from 2 and becomes negative.

13.2.4 Energy Levels in a 2DEG

In a 2D electron gas (2DEG), e.g. in a quantum well or a potential well at a modulation-doped heterointerface, a free motion in z is not possible and k_z is quantized. The energy levels (for each 2D subband) are only given by the cyclotron energy (Fig. 13.12a). The density of states is a sequence of δ-like peaks (Fig. 13.12b). Each peak contributes (degeneracy $\hat{g}$ of a Landau level) a total number of

$$\hat{g} = \frac{e\,B}{h} \tag{13.36}$$

states (per unit area without spin degeneracy and without the degeneracy of the band extremum). In reality, disorder effects lead to an inhomogeneous broadening of these peaks. The states in the tails of the peaks correspond to states that are localized in real space.

Also, in a 2D system several physical properties exhibit an oscillatory behavior as a function of Fermi level, i.e. with varying electron number, and as a function of the magnetic field at fixed Fermi energy, i.e. at fixed electron number (Fig. 13.13).

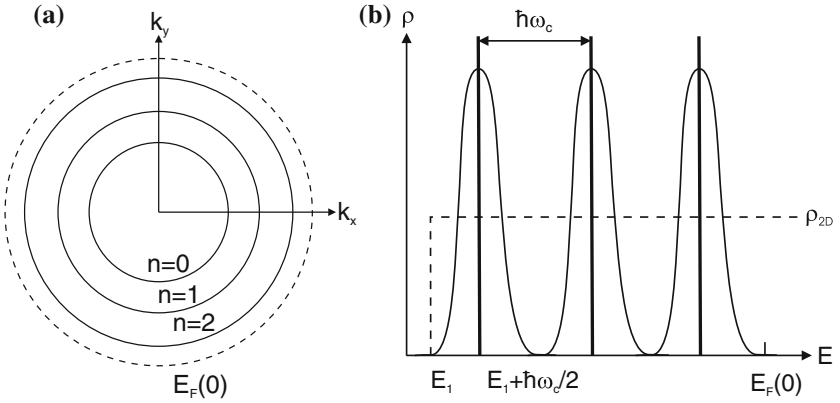

Fig. 13.12 2D electron gas in an external magnetic field. (**a**) Allowed states in **k**-space. (**b**) Density of states (DOS) ρ versus energy. *Dashed line* is two-dimensional DOS without magnetic field. *Thick vertical lines*: δ-like DOS without broadening, *curves*: broadened DOS. Based on [991]

13.2.5 Shubnikov–de Haas Oscillations

From the 2D density of states (per unit area including spin degeneracy) $D^{2D}(E) = m^*/\pi\hbar^2$ the sheet density of electrons n_s can be expressed as a function of the Fermi level (at $T = 0\,\mathrm{K}$ without spin degeneracy)

$$n_s = \frac{m^*}{2\pi\,\hbar^2}\,E_F. \tag{13.37}$$

Using (13.32) we thus find (without spin degeneracy, without valley degeneracy), that the period of $1/B$ is $\propto n_s$:

$$\frac{1}{\Delta B} = \frac{e}{h}\,\frac{1}{n_s}. \tag{13.38}$$

The carrier density of a 2DEG can therefore be determined from the oscillations of magnetoresistance, and is proportional to the density of states at the Fermi level (Shubnikov–de Haas effect). A corresponding measurement with varying field and fixed electron density is shown in Fig. 13.14. The periodicity with $1/B$ is obvious. Since only the component of the magnetic field perpendicular to the layer affects the (x, y) motion of the carriers, no effect is observed for the magnetic field parallel to the layer.

In another experiment the carrier density was varied at constant field (Fig. 13.15). The electron density in an inversion layer in p-type silicon is (linearly) varied with the gate voltage of a MOS (metal–oxide–semiconductor) structure (inset in Fig. 13.15, for MOS diodes cf. Sect. 24.5). In this experiment, the Fermi level was shifted through the Landau levels. The equidistant peaks show that indeed each Landau level contributes the same number of states.

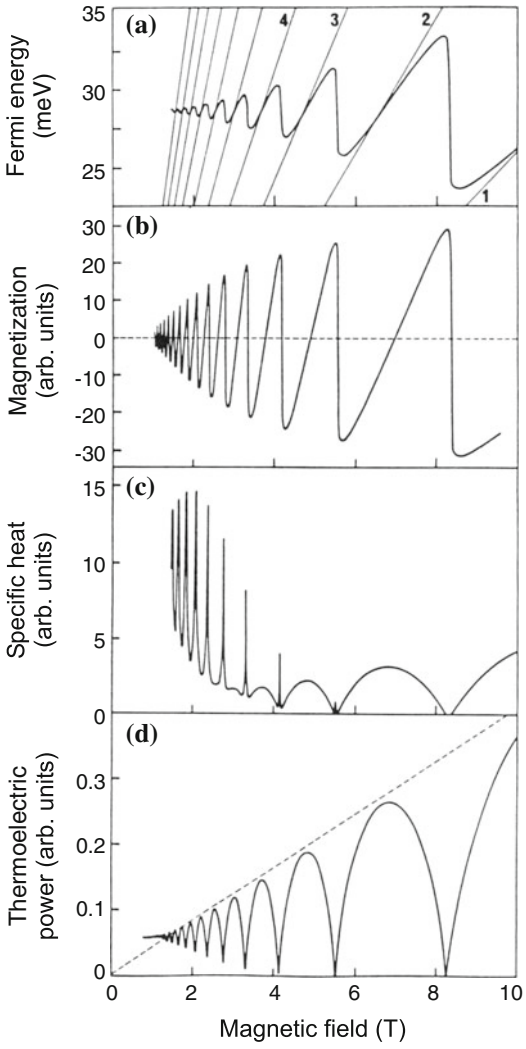

Fig. 13.13 Oscillatory (theory, $T = 6\,\mathrm{K}$) behavior of a 2DEG (GaAs/AlGaAs) in a magnetic field: (**a**) Fermi level, (**b**) magnetization, (**c**) specific heat, (**d**) thermoelectric power. A Gaussian broadening of 0.5 meV was assumed. Adapted from [991, 1111]

13.3 Quantum Hall Effect

In high magnetic fields, at low temperatures and for high-mobility, 2D electron gases exhibit a deviation from the classical behavior. We recall that the classical Hall effect (i.e. considering the Lorentz force, classical Drude theory), the generation of a field E_y perpendicular to a current flow j_x (cf. Sect. 13.2.1), was described with the conductivity tensor $\boldsymbol{\sigma}$ (here, for the (x, y)-plane only)

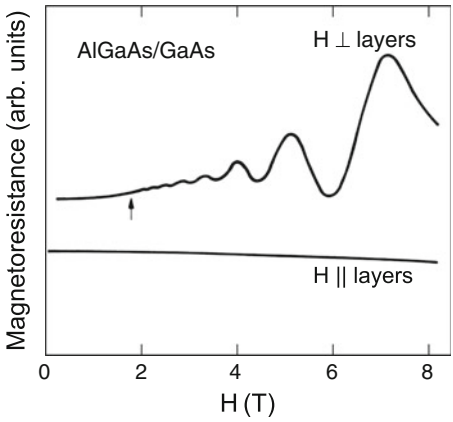

Fig. 13.14 Shubnikov–de Haas oscillations at a modulation-doped AlGaAs/GaAs heterostructure with a 2DEG, $n = 1.7 \times 10^{17}\,\mathrm{cm}^{-2}$ and $\mu = 11\,400\,\mathrm{cm}^2/\mathrm{Vs}$. Data from [1112]

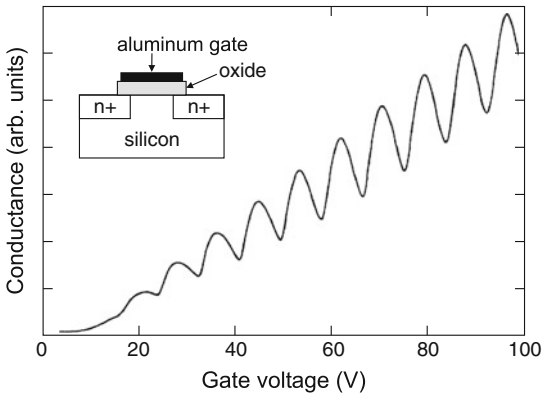

Fig. 13.15 Shubnikov–de Haas oscillations of a 2DEG at the (100) surface of p-type silicon (100 Ω cm) at a magnetic field of 33 kOe and $T = 1.34\,\mathrm{K}$. The *inset* shows schematically the contact geometry. Data from [1113]

$$\boldsymbol{\sigma} = \frac{\sigma_0}{1+\omega_\mathrm{c}^2\tau^2}\begin{pmatrix} 1 & \omega_\mathrm{c}\tau \\ -\omega_\mathrm{c}\tau & 1 \end{pmatrix} \tag{13.39a}$$

$$\sigma_{xx} = \sigma_0 \frac{1}{1+\omega_\mathrm{c}^2\tau^2} \to 0 \tag{13.39b}$$

$$\sigma_{xy} = \sigma_0 \frac{\omega_\mathrm{c}\tau}{1+\omega_\mathrm{c}^2\tau^2} \to \frac{n\,e}{B}\,, \tag{13.39c}$$

where σ_0 is the zero-field conductivity $\sigma_0 = ne^2\tau/m^*$ (8.5). The arrows denote the limit for $\omega_\mathrm{c}\tau \to \infty$, i.e. large fields. The resistivity tensor $\boldsymbol{\rho} = \boldsymbol{\sigma}^{-1}$ is given by

$$\boldsymbol{\rho} = \begin{pmatrix} \rho_{xx} & \rho_{xy} \\ -\rho_{xy} & \rho_{xx} \end{pmatrix} \tag{13.40a}$$

$$\rho_{xx} = \frac{\sigma_{xx}}{\sigma_{xx}^2 + \sigma_{xy}^2} \to 0 \tag{13.40b}$$

$$\rho_{xy} = \frac{-\sigma_{xy}}{\sigma_{xx}^2 + \sigma_{xy}^2} \rightarrow -\frac{B}{n\,e}. \tag{13.40c}$$

13.3.1 Integral QHE

Experiments yield strong deviations from the linear behavior of the transverse resistivity $\rho_{xy} = E_y/j_x = BR_H$ with the Hall coefficient $R_H = -1/(ne)$ with increasing magnetic field is observed at low temperatures for samples with high carrier mobility, i.e. $\omega_c\tau \gg 1$ (Fig. 13.16). In Fig. 13.17a,b, Hall bars are shown for 2DEGs in silicon metal–oxide–semiconductor field-effect transistor (Si-MOSFET) electron inversion layers and at GaAs/AlGaAs heterostructures, respectively.

The Hall resistivity exhibits extended Hall plateaus with resistivity values that are given by

$$\rho_{xy} = \frac{1}{i}\,\frac{h}{e^2}\,, \tag{13.41}$$

i.e. integer fractions of the quantized resistance $\rho_0 = h/e^2$ =25812.807… Ω, which is also called the von-Klitzing constant. In Fig. 13.16, a spin splitting is seen for the $n = 1$ Landau level (and a small one for the $n = 2$). We note that the topmost Hall

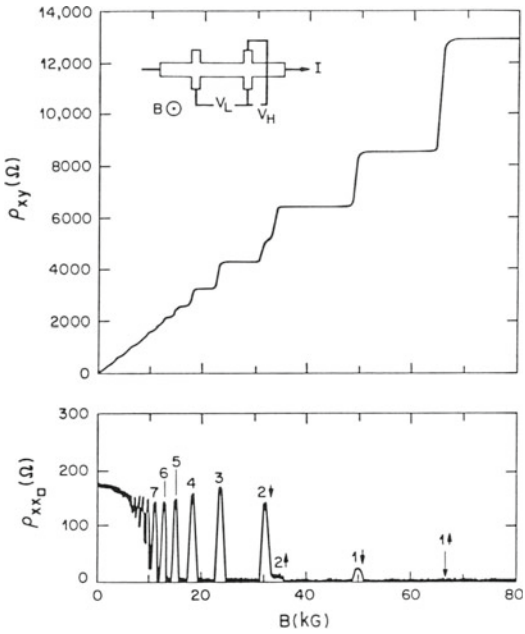

Fig. 13.16 Hall resistivity ρ_{xy} and longitudinal resistivity ρ_{xx} for a modulation-doped GaAs/AlGaAs heterostructure ($n = 4 \times 10^{11}\,\mathrm{cm}^{-2}$, $\mu = 8.6 \times 10^4\,\mathrm{cm}^2/\mathrm{Vs}$) at 50 mK as a function of magnetic field (10 kG=1 T). The numbers refer to the quantum number and spin polarization of the Landau level involved. The inset shows schematically the Hall bar geometry, V_L (V_H) denotes the longitudinal (Hall) voltage drop. Reprinted with permission from [1114], ©1982 APS

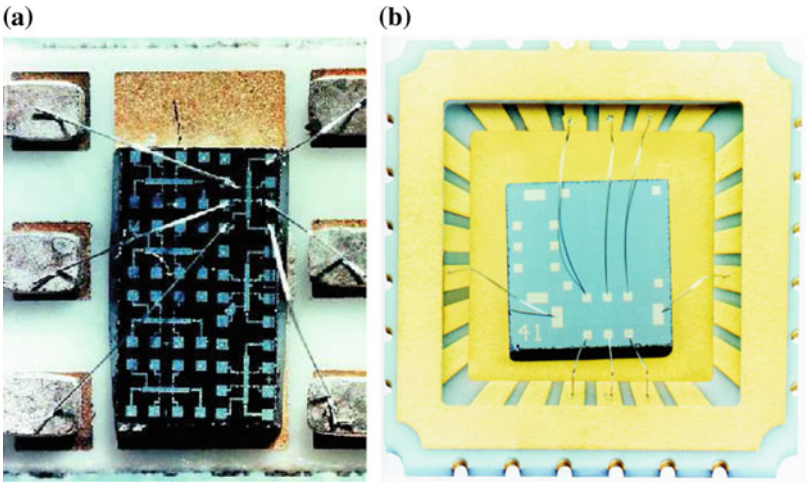

Fig. 13.17 (**a**) Silicon MOS (metal–oxide–semiconductor) structure of K. v. Klitzing's et al. original experiments. (**b**) GaAs/AlGaAs heterostructure sample grown with molecular beam epitaxy for QHE measurements, chip carrier and bond wires. Reprinted with permission from [1115]

plateau is due to the completely filled $n = 0$ Landau level; the resistance is $\rho_0/2$ due to the spin degeneracy of 2.

The integral quantum Hall effect, first reported in [1116, 1117], and the value for ρ_0 are found for a wide variety of samples and conditions regarding sample temperature, electron density or mobility of the 2DEG and the materials of the heterostructure.

Within the plateau the resistivity is well defined within 10^{-7} or better up to 4×10^{-9}. A precise determination allows for a new normal for the unit Ohm [1118, 1119], being two orders of magnitude more precise than the realization in the SI system, and an independent value for the fine-structure constant $\alpha = \frac{e^2}{\hbar c}\frac{1}{4\pi\epsilon_0}$. At the same time, the longitudinal resistivity, starting from the classical value for small magnetic fields, exhibits oscillations and eventually it is zero for the plateaus in ρ_{xy}. For ρ_{xx} values of $10^{-10}\,\Omega/\square$ have been measured, which corresponds to $10^{-16}\,\Omega$/cm for bulk material, a value three orders of magnitude smaller than for any nonsuperconductor.

The interpretation of the quantum Hall effect(s) is discussed in [1120] among many other treatises. The simplest explanation is that the conductivity is zero when a Landau level is completely filled and the next is completely empty, i.e. the Fermi level lies between them. The temperature is small, i.e. $kT \ll \hbar\omega_c$, such that no scattering between Landau levels can occur. Thus no current, similar to a completely filled valence band, can flow. The sheet carrier density n_s is given by counting the i filled Landau levels (degeneracy according to (13.36)) as

$$n_s = i\,\frac{eB}{h}. \tag{13.42}$$

In the transverse direction energy dissipation takes place and the Hall resistivity $\rho_{xy} = B/(n_s e)$ takes the (scattering-free) values given in (13.41).

However, this argument is too simple as it will not explain the extension of the plateaus. As soon as the system has one electron more or less, the Fermi energy will (for a system with δ-like density of states) be located in the upper or lower Landau level, respectively. Then, the longitudinal conductivity should no longer be zero and the Hall resistivity deviates from the integer fraction of ρ_0.

Therefore (in the localization model) an inhomogeneous (Gaussian) broadening of the density of states is assumed. Additionally, the states in the tails of the distribution are considered nonconducting, i.e. localized, while those around the peak are considered conductive. This mobility edge is schematically shown in Fig. 13.18a–c.

When the Fermi level crosses the density of states of the broadened Landau level (upon increase of the magnetic field), it first populates localized states and ρ_{xx} remains at zero. When the Fermi level crosses the delocalized, conducting states, the longitudinal conductivity shows a peak and the Hall conductivity increases from the plateau value by e^2/h to the next plateau. When the Fermi level lies within the upper nonconducting states, the Hall resistivity remains constant in the next plateau. For the sample in Fig. 13.16 it has been estimated that 95 % of the Landau level states are localized [1114].

In the localization model it is still astonishing that the samples exhibit the step of e^2/h in the conductivity as if *all* electrons on the Landau level contribute to conduction, cf. (13.42). According to the calculations in [1123] the Hall current lost by the localized states is compensated by an extra current by the extended states. The behavior of the electrons in the quantum Hall regime ('quantum Hall liquid') can be considered similar to that of an incompressible fluid where obstructions lead the fluid to move with increased velocity. Nevertheless, the single particle picture seems to be insufficient to model the IQHE.

Another model for the explanation of the QHE, supported now with plenty of experimental evidence, is the edge state model where quantized one-dimensional conductivity of edge channels, i.e. the presence of conductive channels along the sample boundaries, is evoked [1124]. Due to depletion at the boundary of the sample, the density of the 2DEG varies at the edge of the sample and 'incompressible' stripes develop for which $\partial\mu/\partial n_s \to \infty$. When the filling factor is far from an integer, the Hall voltage is found to vary linearly across the conductive channel and the current is thus homogeneous over the sample (Fig. 13.18d). In the Hall plateau, the Hall voltage is flat in the center of the channel and exhibits drops at the edges, indicating that the current flows along the boundary of the sample (edge current) [1122] in agreement with predictions from [1125]. Although the current pattern changes with varying magnetic field, the Hall resistivity remains at its quantized value.

The most fundamental arguments for the explanation of the IQHE come from gauge invariance and the presence of a macroscopic quantum state of electrons and magnetic flux quanta [1126]. This model holds as long as there are any extended states at all.

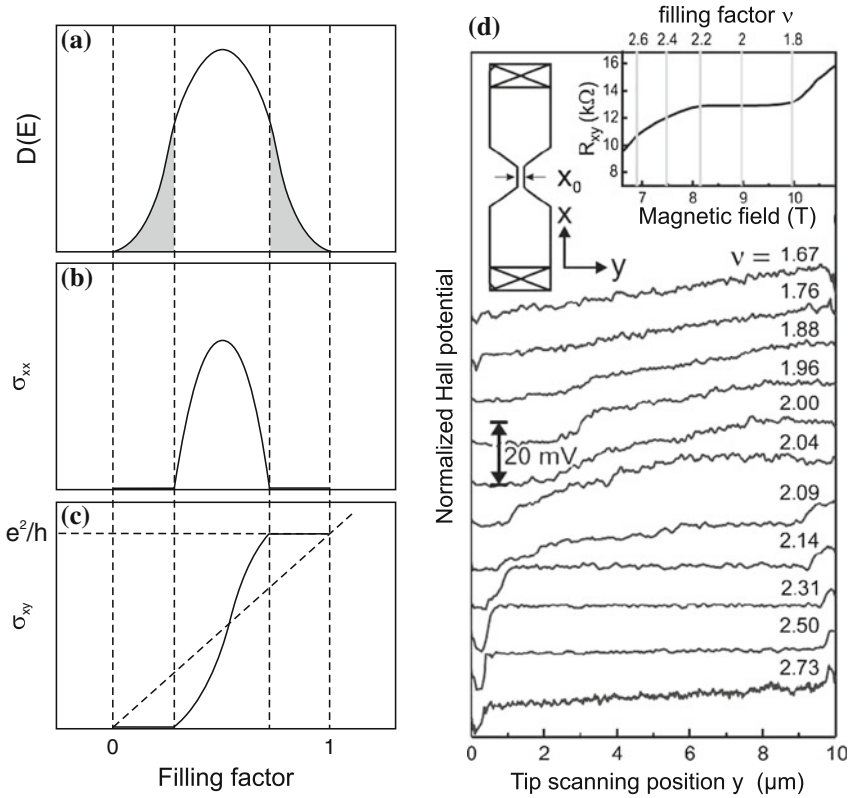

Fig. 13.18 (**a**) Density of states $D(E)$, (**b**) longitudinal conductivity σ_{xx} and (**c**) Hall conductivity σ_{xy} for a Landau level as a function of the filling factor $\mu = n/d$, where n is the electron density and d the degeneracy of the level. In (**a**) the filling factor relates via the position of the Fermi level to an energy scale. The *grey areas* in (**a**) denote localized states. The *slanted dashed line* in (**c**) has a slope of ne/B. Adapted from [1121]. (**d**) Normalized Hall potential profile for different magnetic fields around filling factor $\nu = 2$. The overall voltage drop corresponds to 20 mV. The *insets* show the sample geometry and transport data. The 2DEG is from a GaAs/$Al_{0.33}Ga_{0.67}$As modulation-doped heterostructure, $n_s = 4.3 \times 10^{11}\,\mathrm{cm}^{-2}$, $\mu = 5 \times 10^5\,\mathrm{cm}^2/\mathrm{Vs}$, $T = 1.4\,\mathrm{K}$. Adapted from [1122]

13.3.2 Fractional QHE

For very low temperatures and in the extreme quantum limit, novel effects are observed when the kinetic energy of the electrons is smaller than their Coulomb interaction. New quantum Hall plateaus are observed at various fractional filling factors $\nu = p/q$. We note that the effects of the fractional quantum Hall effect (FQHE) in Fig. 13.19 mostly arise for magnetic fields beyond the $n = 1$ IQHE plateau. The filling factor $\nu = n/(eB/h)$ is now interpreted as the number of electrons per magnetic flux quantum $\phi_0 = h/e$.

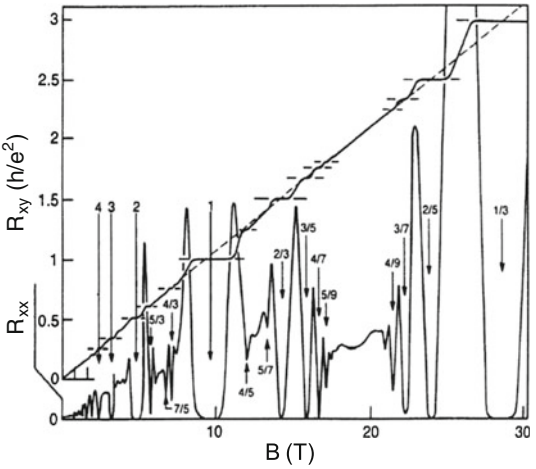

Fig. 13.19 Hall resistance R_{xy} and magnetoresistance R_{xx} of a two-dimensional electron system (GaAs/AlGaAs heterostructure) of density $n = 2.33 \times 10^{11}\,\mathrm{cm}^{-2}$ at a temperature of 85 mK, versus magnetic field B. Numbers identify the filling factor ν, which indicates the degree to which the sequence of Landau levels is filled with electrons. Plateaus are due to the integral ($\nu = i$) quantum Hall effect (IQHE) and fractional ($\nu = p/q$) quantum Hall effect (FQHE). Adapted from [1127], reprinted with permission, ©1990 AAAS

The effects of the FQHE cannot be explained by single-electron physics. The plateaus at fractional fillings ν occur when the Fermi energy lies within a highly degenerate Landau (or spin) level and imply the presence of energy gaps due to many-particle interaction and the result of correlated 2D electron motion in the magnetic field.

A decisive role is played by the magnetic flux quanta. The presence of the magnetic field requires the many-electron wavefunction to assume as many zeros per unit area as there are flux quanta penetrating it. The decay of the wavefunction has a length scale of the magnetic length $l_0 = \sqrt{\hbar/(eB)}$. Since the magnetic field implies a 2π phase shift around the zero, such an object is also termed a *vortex*, being the embodiment of the magnetic flux quanta in the electron system. Such a vortex represents a charge deficit (compared to a homogeneous charge distribution) and thus electrons and vortices attract each other. If a vortex and an electron are placed onto each other, considerable Coulomb energy is gained. At $\nu = 1/3$, there are three times more vortices than there are electrons, each vortex representing a charge deficit of $1/3\,e$. Such a system is described with many-particle wavefunctions, such as the Laughlin theory for $\nu = 1/q$ [1126] and novel quasi-particles called *composite fermions*[1128, 1129] for other fractional fillings. For further reading we refer readers to [1130]and references therein.

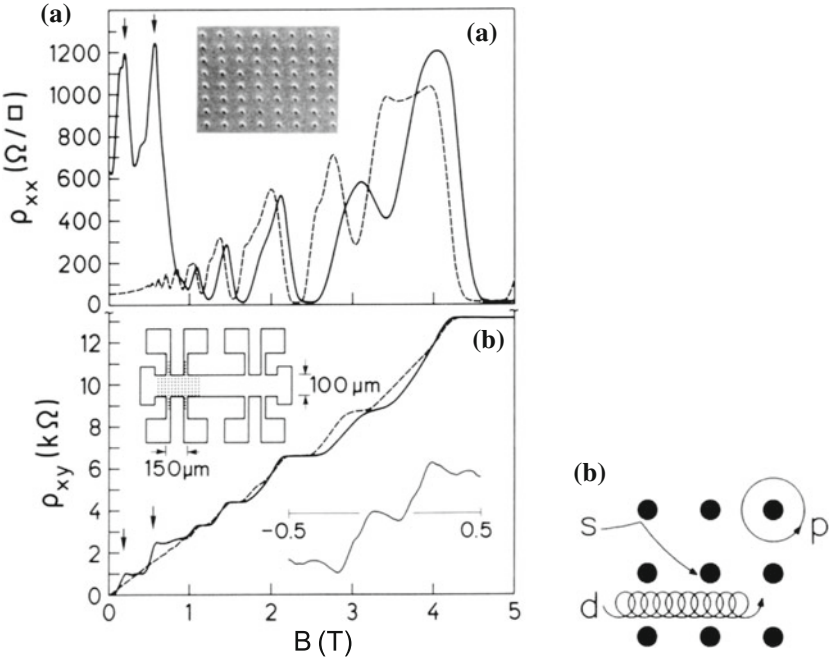

Fig. 13.20 Weiss oscillations: (**a**) magnetoresistance and (**b**) Hall resistance of an antidot lattice (*inset* in (**a**)) with pattern (*solid lines*) and without pattern (*dashed lines*) at $T = 1.5\,\mathrm{K}$. (**b**) Schematic of the different orbits: ('p': pinned, 'd': drifting, 's': scattered). Reprinted with permission from [1131], ©1991 APS

13.3.3 Weiss Oscillations

In Fig. 13.20, measurements are shown for a Hall bar in which an array of antidots (in which no conduction is possible) has been introduced by dry etching. The antidot size is 50 nm (plus depletion layer) and the period is 300 nm. These obstructions for the cyclotron motion lead to a modification of the magnetotransport properties.

Before etching of the antidot array the 2DEG has a mean free path length of 5–10 μm at 4 K for the mobility of $\approx 10^6\,\mathrm{cm}^2/\mathrm{Vs}$. At low magnetic fields there is a strong deviation of the Hall resistivity from the straight line to which the QHE levels converge. Similarly, ρ_{xx} shows a strong effect as well.

These effects are related to commensurability effects between the antidot lattice and the cyclotron resonance path. When the cyclotron orbit is equal to the lattice period, electrons can fulfill a circular motion around one antidot (pinned orbit, Fig. 13.20b) that leads to a reduction of conductivity. At high fields, drifting orbits for which the cyclotron orbit is much smaller than the lattice period occur. At small fields, scattering orbits also contribute for which the cyclotron radius is large and the electron has antidots from time to time. Resonances in the Hall resistivity have been found due to pinned orbits enclosing 1, 2, 4, 9 or 21 antidots.